#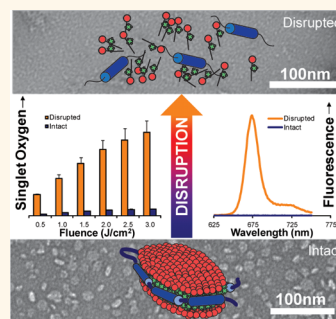 Self-Assembled Porphyrin Nanodiscs with Structure-Dependent Activation for Phototherapy and Photodiagnostic Applications

Kenneth K. Ng,[†,‡] Jonathan F. Lovell,[†,‡,||] Ali Vedadi,[‡,§] Taraneh Hajian,[§] and Gang Zheng[†,‡,⊥,*]

[†]Institute of Biomaterials and Biomedical Engineering, University of Toronto, Toronto, Canada, [‡]Ontario Cancer Institute, Campbell Family Cancer Research Institute and Techna Institute, University Health Network, Toronto, Canada, [§]Ontario Structural Genomics Consortium, University of Toronto, Toronto, Canada, and [⊥]Department of Medical Biophysics, University of Toronto, Toronto, Canada. [||]Present address: Department of Biomedical Engineering, University at Buffalo, State University of New York, United States.

ABSTRACT The abilities to deliver and subsequently activate a therapeutic at the intended site of action are two important challenges in the synthesis of novel nanoparticles. Poor tumor permeability as a result of a dense microenvironment can impede the delivery of nanoparticles to the site of action. The design of a sub-40 nm activatable porphyrin nanodisc, based on protein-induced lipid constriction, is described. The biophotonic nanoparticle, self-assembled from aggregated porphyrin—lipid, is stabilized by an amphipathic alpha helical protein and becomes photoactive when its structure is perturbed. Enzymatic cleavage of the constricting protein leads to conversion of the particle from a disc- to a vesicle-shaped structure and provides further evidence that the apolipoprotein serves a functional role on the nanodisc. Fluorescence measurements of these nanodiscs in a detergent show that fluorescence is over 99% quenched in the intact state with a 12-fold increase in singlet oxygen generation upon disruption. Cellular fluorescence unquenching and dose-dependent phototoxicity demonstrate that these nanodiscs can be internalized and unquenched intracellularly. Finally, nanodiscs were found to display a 5-fold increase in diffusion coefficient when compared with the protein-free control (($3.5 \pm 0.1) \times 10^{-7}$ *vs* $(0.7 \pm 0.03) \times 10^{-7}$ cm^2 s^{-1}). The ability to incorporate large amounts of photosensitizer drugs into its compact structure allows for phototherapeutic action, fluorescence diagnostic applications, and the potential to effectively deliver photosensitizers deep into poorly permeable tumors.

KEYWORDS: porphyrin · nanodisc · self-assembly · activation · drug delivery · porphysome

The design of novel materials for application in nanomedicine holds the key to drug delivery in the future. The study of molecular self-assembly whereby molecules self-associate in solution through weak intermolecular forces has allowed for exquisite control over nanoparticle size, geometry, and surface chemistry. This is especially important when designing multicomponent and multifunctional nanoparticles.[1] Moreover, by coupling dynamic structural changes with photophysical phenomena that occur at the nanometer length scale, activatable nanoparticles can be designed. Upon activation by external stimuli, these "smart" agents can undergo changes at the nanoscale to elicit an effect. The concept of nanoparticles that activate due to external stimulus will have useful applications in photodynamic therapy and photodiagnosis. In these two scenarios, the degree of success is dependent on preferential accumulation of the photoactive agent into target *versus* normal tissues. By activating the agent only in the target, an additional layer of specificity can be included into the treatment process. A physical phenomenon that is highly amenable to the design of a "smart" agent is the aggregate-induced fluorescence quenching mechanism. Various groups have taken advantage of this mechanism to generate activatable therapeutics.[2−4] In particular, recent work by Lovell *et al.* showed that stable biophotonic nanostructures (>100 nm) can be prepared by conjugating pyropheophorbide, a reduced porphyrin, to the glycerol backbone of lysophospholipids
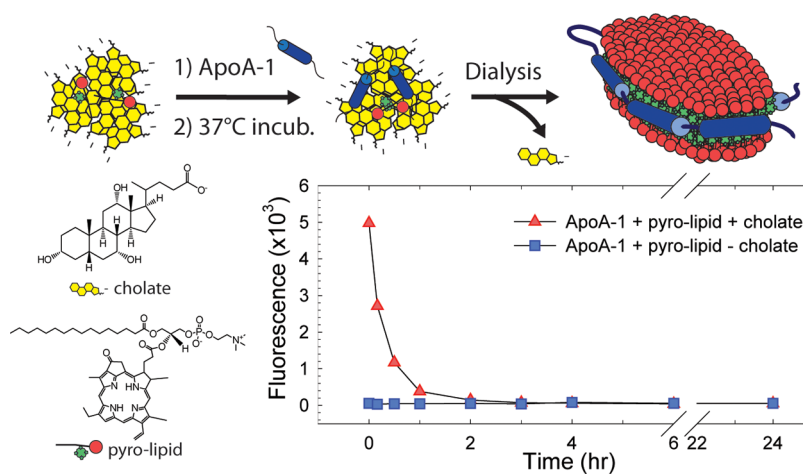
©2013 American Chemical Society

Figure 1. Detergent dialysis procedure used to prepare porphyrin nanodiscs. Removal of the detergent facilitates the self-assembly of the nanoparticle, which can be followed by monitoring fluorescence quenching.
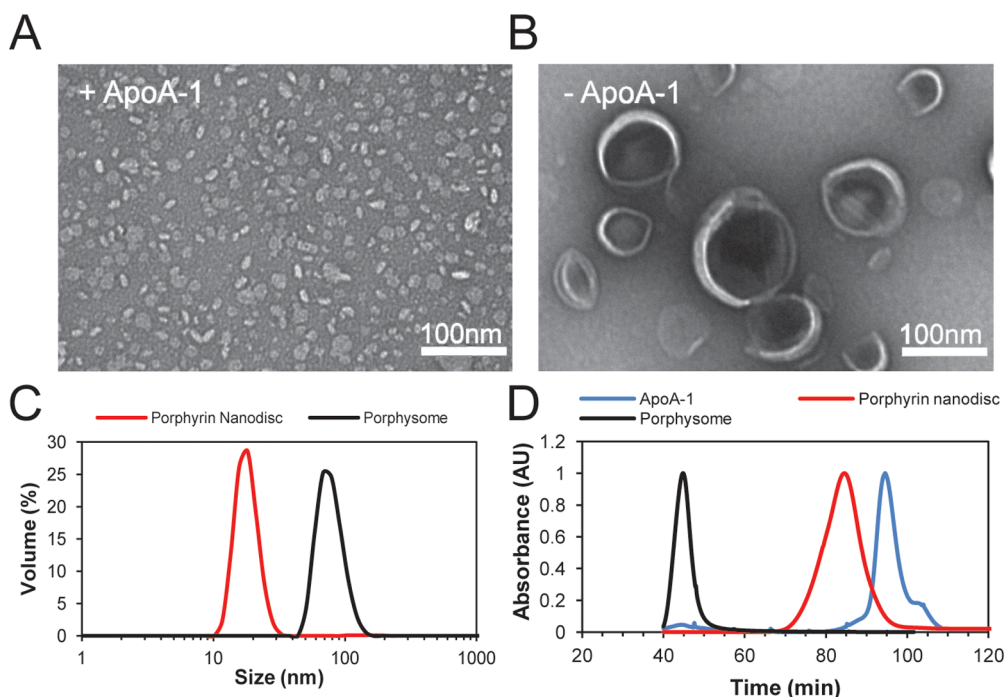

Figure 2. Characterization of products synthesized from detergent dialysis. (A) Transmission electron micrographs of nanoparticles synthesized in the presence of ApoA-1. (B) Transmission electron micrographs of nanoparticles synthesized in the absence of ApoA-1. (C) Dynamic light scattering measurements of nanoparticles synthesized in the presence (porphysomes) and absence (nanodiscs) of ApoA-1. (D) Size exclusion chromatograph illustrating the molecular weight differences between porphysomes, nanodiscs, and ApoA-1 alone. All scale bars represent 100 nm.

(pyro-lipid).[5,6] This lipid conjugate is fluorescent, can generate singlet oxygen, and can stably chelate metals for radioimaging applications.[7] When mechanically formulated, the porphyrin nanovesicles (porphysomes) generated exhibit fluorescence quenching and photothermal properties[8] and adopt a kinetically stable size of >100 nm.

While nanoparticles in the 100−200 nm size range can accumulate in cancer tumors through the enhanced permeation and retention effect, the local tumor environment may influence the depth of penetration.[9] Recent studies have shown that nanoparticles less than 40 nm may be more effective at penetrating deeply into fibrous tumors than their larger counterparts.[10,11] Attempts to create smaller pyro-lipid vesicles remain a challenge due to growing instability as a result of the surface curvature. Indeed, past studies conducted on dipalmitoylphosphatidylcholine vesicles have shown that sub-40 nm vesicles are unstable due to their tendency to spontaneously fuse below their transition temperature. To generate bilayer structures smaller than this size,[12] one strategy is to integrate amphiphiles with non-cone-like geometries to facilitate assembly into nonspherical kinetically stable structures.

In this manner, adjacent pyro-lipid molecules may retain their tight packed structure within the nanoparticle. The apolipoprotein is an example of such an amphiphile. Aqueous solutions of apolipoproteins form amphipathic α-helical structures that interact rapidly with phospholipids to generate discoidal structures. In nature, such apolipoproteins complex phospholipids in the body and serve a critical function in cholesterol transport. *In vitro*, apolipoproteins and their mimetics have been used to solubilize phospholipids for a host of applications including structural biology,[13,14] molecular imaging,[15] and drug delivery.[16−19] To recapitulate the properties of reversibly quenched porphyrin aggregates in a smaller nanoparticle, a strategy involving lipid constriction by amphipathic alpha helical proteins was pursued. Since class A amphiphilic alpha helical proteins have been known to stabilize patches of phospholipid in a belt-like manner, it was posited that such protein interactions with pyro-lipid will maintain the tight phospholipid packing required for quenching, while the presence of the labile protein will facilitate nanoparticle activation upon proteolysis after uptake.

RESULTS AND DISCUSSION

Nanodiscs were prepared using the detergent dialysis procedure as originally reported by Matz and Jonas in their synthesis of reconstituted high-density lipoproteins.[20] In a typical formulation, a lipid film was prepared by drying a methanol solution of pyro-lipid (133 nmol) in a glass test tube under a continuous stream of nitrogen, followed by vacuum desiccation. A sodium cholate solution (20 mM) in a 75× mole excess was applied to rehydrate the film. This was followed by the addition of apolipoprotein A-1 (ApoA-1; 5.3 nmol). Rehydrating the film with the detergent yielded a highly fluorescent solution, which indicated that cholate completely solubilized pyro-lipid into well-separated monomers (Figure 1). The mixture was incubated at 37 °C overnight (~16 h) to ensure maximal binding between the protein and the pyro-lipid/cholate mixture. After incubation, the sample was exhaustively dialyzed at 4 °C for 24 h with three buffer changes. Each buffer change occurred at a 1000-fold buffer-to-sample ratio. As the dialysis procedure progressed under sink conditions, cholate was removed slowly, facilitating assembly of nanoscale structures. By monitoring the fluorescence quenching over time, it was possible to indirectly monitor cholate removal and the resultant aggregate packing of pyro-lipid (Figure 1).

The product formed from the dialysis reaction was characterized by transmission electron microscopy (TEM), dynamic light scattering (DLS), and size exclusion chromatography (SEC). When ApoA-1 was added to the formulation process, small elliptical and spherical structures were observed that were between 10 and 30 nm in size (Figure 2A). We hypothesized that the
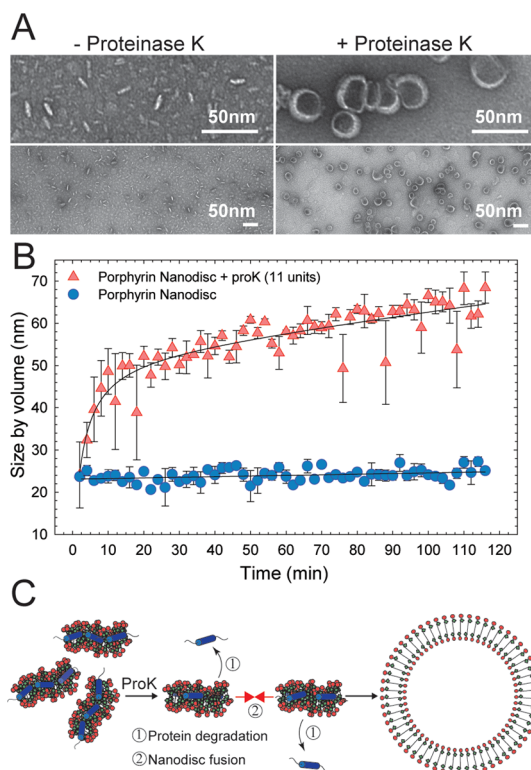

Figure 3. Influence of apolipoprotein on nanodisc structure probed by protease degradation. (A) Transmission electron micrographs of nanodiscs with no treatment (left) or treatment (right) with proteinase K (11 units). Scale bars represent 50 nm. (B) Kinetics of nanodisc size change in samples treated with or without proteinase K over a period of 2 h. Data represent the mean ± standard error of the mean of three independent trials. (C) Proposed mechanism of size and morphological change in protein nanodiscs.

elliptical and spherical structures were the edge-on and face-on projections of the same particle, respectively. These observations have also been reported by other groups studying apolipoprotein-bound phospholipid particles.[21] In contrast to the ApoA-1-containing sample, nanostructures formed in the absence of ApoA-1 had morphologies reminiscent of porphysomes (Figure 2B). Comparing the size distributions generated from DLS (Figure 2C) and SEC (Figure 2D) measurements, we found nanodiscs to be smaller than the sample prepared without the apolipoprotein. Furthermore, size exclusion data showed that free protein eluted from the column at a later time compared to the nanodiscs, indicating that the observed size change was not due to the presence of free protein.

In addition to ApoA-1, additional types of amphipathic α-helical proteins were tested during formulation to establish whether the interaction between the protein and pyro-lipid could be extended to additional class A amphiphatic α-helical proteins.[22] It was found that apolipoprotein E3 (ApoE3) and membrane scaffold protein 1E3D1 (MSP1E3D1) could interact with pyro-lipid to form similar nanodisc structures (Figure S1).
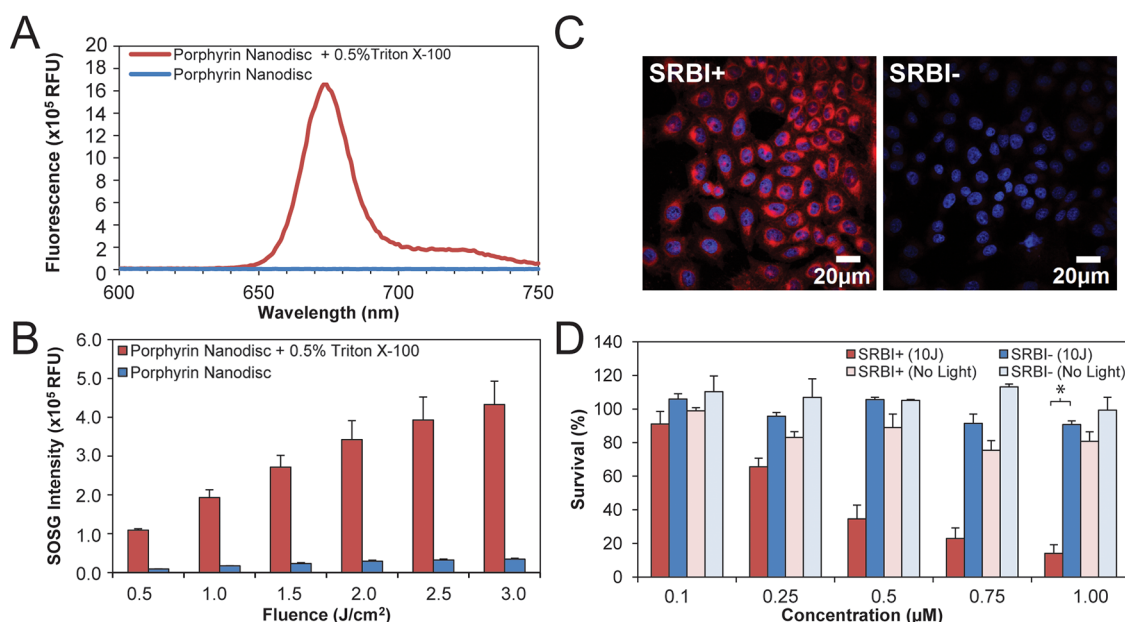
Figure 4. Characterization of *in vitro* activatable fluorescence and photodynamic activity. (A) Fluorescence emission of nanodiscs in the intact (blue) *versus* the disrupted (red) state. (B) Singlet oxygen generation upon light irradiation (660 nm; 1.7 mW cm^{-2}) reported by the singlet oxygen sensor (6 μM) of nanodiscs (1 μM) in the intact (blue) *versus* the Triton X-100 disrupted (red) state. Data represent the mean $\pm$ standard deviation of three independent trials. (C) Nanodisc uptake in a model CHO cell line expressing (left) and not expressing (right) SRBI, a receptor that interacts with ApoA-1. The scale bars represent 20 μm. (D) Effect of nanodisc concentration on light (660 nm; 1.7 mW cm^{-2})-induced phototoxicity in SRBI^{+} (red) and SRBI^{-} (blue) cells. Data represent the mean $\pm$ standard error of the mean of three independent trials.

To further confirm that the size and morphology of the nanodisc was influenced by the interactions with the apolipoprotein, nanodiscs were subjected to protease degradation by proteinase K. Porphyrin nanodiscs synthesized using ApoE3 was incubated with proteinase K (11 units) at 37 °C, and changes in size and shape were monitored by TEM and DLS. It was found that after a 2 h digestion the nanoparticles reverted from a disc to a vesicle-like structure (Figure 3A). When we examined the time course of this process by DLS, we found that the size of the vesicles rapidly increased to 50 nm within the first 10 min, followed by a slower increase over the remainder of the experiment (Figure 3B). Size and shape changes were not observed in the discs incubated at 37 °C in the absence of protease, indicating that nanodiscs were stable at physiological temperatures. The process of disc-to-vesicle conversion in phospholipids has previously been the focus of several studies.[23,24] The conversion from disc to vesicle initiated by proteinase K likely involves cleavage and dissociation of the apolipoprotein, followed by enlargement through disc-to-disc fusion and finally closure to generate the resultant vesicle structure (Figure 3C).

Examining the photophysical properties of the nanodisc, we observed that fluorescence was quenched in the intact particle but was successfully liberated when the packed structure of the nanodisc was disrupted with a 0.5% solution of Triton X-100. The degree of fluorescence quenching was found to be 0.99. To determine the relative amount of singlet oxygen

generated in the porphyrin nanodiscs in the native and disrupted states, we employed Singlet Oxygen Sensor Green (SOSG), a selective $^1O_2$ fluorescent reporter.[25] Both samples were adjusted to the same pyro-lipid concentration and then irradiated with 3.0 J/cm^2 of light at 660 nm. When irradiated, samples of disrupted nanodiscs generated approximately 12 times more singlet oxygen than the native nanodiscs as measured by changes in SOSG fluorescence (Figure 4B).

The activatable nature of porphyrin nanodiscs may be suited for imaging and photodynamic therapy. To probe these properties, porphyrin nanodisc uptake studies were conducted in a pair of Chinese hamster ovary (CHO) cell lines: one, transfected (SRBI^{+}), and, the other, untransfected (SRBI^{-}) with the scavenger receptor class B type I. This receptor has previously been shown to interact with the ApoA-1 protein in the lipid-bound state and is used in this experiment to efficiently facilitate uptake of the nanodiscs into the cells.[26] Both cell lines were incubated with porphyrin nanodiscs at a pyro-lipid concentration of 2.4 μM. Confocal images of each cell line showed that SRBI^{+} cells were able to internalize and unquench nanodiscs, presumably through a mechanism that disrupted the nanodisc structure (Figure 4C). To investigate the effect of light treatment on CHO cell lines, cells were incubated with varying concentrations of porphyrin nanodiscs and treated with either 0 or 10 J of 660 nm light (Figure 4D). Cells expressing the SRBI^{+} receptor experienced a dose-dependent decrease in survival when treated with light. In contrast, SRBI^{-} cells did not show
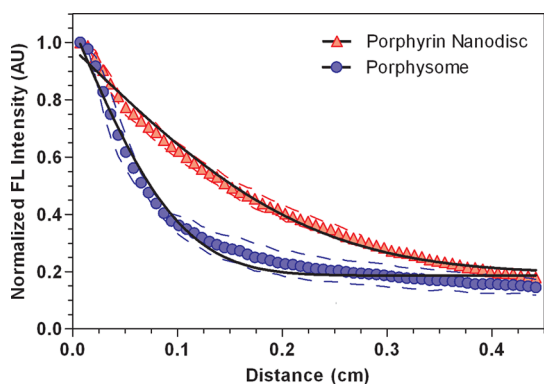
Figure 5. Diffusion of ApoA-1-containing nanodiscs (red triangles, diffusion coefficient $(3.5 \pm 0.1) \times 10^{-7}$ cm^2 s^{-1}) *versus* ApoA-1-absent porphysomes (blue circles, $(0.7 \pm 0.03) \times 10^{-7}$ cm^2 s^{-1}) through a collagen gel (7.4 mg mL^{-1}) at 37 °C over a period of 16 h. Data points represent the mean $\pm$ standard deviation of three independent trials. The solid black lines are theoretical fits of the data to a one-dimensional diffusion model.

any dose response effect when treated with nanodiscs and irradiated with light. Furthermore, there was no significant cell death when porphyrin nanodiscs were incubated with the cells that did not undergo light treatment.

The size and shape of a nanoparticle may have an effect on tumor penetration especially in collagen-rich and/or poorly permeable tumors.[10] Studies on a series of quantum dot (QD)-based nanoparticles showed that 12 nm QDs had the greatest penetration through a Mu89 melanoma model as compared with the 60 nm and 125 nm size nanoparticles.[27] Furthermore, non-spherical geometries such as rod-shaped nanoparticles have been demonstrated to permeate deeper through orthotopic E0771 mammary tumors greater than their spherical counterparts with equal average hydrodynamic size.[28] To examine whether ApoA-1-stabilized pyro-lipid can increase the penetration of the nanoparticle through a collagen-rich environment, a collagen permeability assay was conducted. In this experiment the diffusion of porphyrin nanodiscs was compared with porphysomes, synthesized in the absence of ApoA-1. A collagen gel at a concentration (7.4 mg/mL) that mimicked the collagen content of poorly permeable tumors (*i.e.*, colon adenocarcinoma, mammary carcinoma) was prepared.[29,30] To this gel, nanodiscs or porphysomes (200 μM) labeled with a near-infrared tracer (bacteriochlorophyll—lipid) were applied, incubated at 37 °C for 14 h, and promptly imaged by a hyperspectral fluorescence imager (ex 671—705 nm; em 790 nm). Line profiles of fluorescence were measured using ImageJ, and the fluorescence as a function of distance was plotted (Figure 5). Data were fit using a one-dimensional diffusion model to calculate the apparent diffusion coefficient of each nanoparticle in the collagen gel. The apparent diffusion coefficients calculated using this method were $(3.5 \pm 0.1) \times 10^{-7}$ cm^2 s^{-1} ($R^2 = 0.9866$) for the porphyrin nanodiscs and $(0.7 \pm 0.03) \times 10^{-7}$ cm^2 s^{-1} ($R^2 = 0.9613$) for porphysomes. These results indicate that nanodiscs have a greater capability of diffusing through a tumor's collagen rich matrix when compared with porphysomes and can be attributed to its smaller hydrodynamic radius, which enables less inhibited diffusion through the collagen matrix.

CONCLUSION

In summary, activatable porphyrin nanodiscs were synthesized by complexing apolipoproteins to pyro-lipid using the detergent dialysis method. These nanodiscs varying from 10 to 30 nm in size had a disc-like morphology when compared with the larger porphysomes. Disruption of the nanodisc structure increased both the fluorescence and the singlet oxygen generation in the discs, while the utility of this nanoparticle was demonstrated in an *in vitro* model. Finally, the potential improvement in penetration in permeable tumors was demonstrated by examining the diffusive properties of the nanodiscs in a collagen-rich environment.

MATERIALS AND METHODS

Materials. Pyropheophorbide-conjugated lipid (pyro-lipid) was synthesized as previously described.[5] Sodium cholate dihydrate was purchased from Sigma-Aldrich (St. Louis, MO). Regenerated cellulose dialysis membrane was purchased from Fisher Scientific (Ottawa, ON). Carbon-coated copper transmission electron microscopy grids were purchased from Canemco (Lakefield, QC). The plasmid coding for recombinant was received as a gift from Dr. Sissel Lund-Katz. Membrane scaffold protein 1E3D1 was received as a gift from Dr. Stephen Sligar. BL21-V2R *Escherichia coli* (*E. coli*) cells were purchased from New England BioLabs (Pickering, ON). LB medium was obtained from Difco (Lawrence, KS) as an LB broth. Isopropyl β-D-1 thiogalactopyranoside (IPTG) was purchased from Sigma-Aldrich (St. Louis, MO). Nickel-NTA resin was acquired from Qiagen Canada (Toronto, ON). Imidazole was procured from Sigma-Aldrich. Thrombin was purchased through Sigma-Aldrich as a lyophilized powder isolated from human plasma (St. Louis, MO).

Singlet Oxygen Sensor Green (SOSG) was purchased from Invitrogen (Burlington, ON). Triton X-100 was purchased from Biorad (Mississauga, ON). ldlA7 (SRBI$^-$) and ldlA[mSRBI] (SRBI$^+$) cells were kind gifts from Dr. Monty Krieger. RPMI 1640 was purchased from ATCC (Manassas, VA). Type I rat tail collagen was purchased from BD (Mississauga, ON). Rectangular capillary tubes were purchased from Vitrocom Inc. (Mountain Lakes, NJ).

Isolation and Expression of Alpha Helical Proteins. Apolipoprotein A-1 (A1) was isolated from expired human plasma obtained from the institutional blood transfusion lab.[31] Use of expired plasma was approved by the institution's research ethics board. Expression of recombinant apolipoprotein E3 (E3) was conducted in *E. coli* as previously described in the literature.[32] Briefly *E. coli* BL21 (DE3) pRARE-V2R was transformed with plasmid encoding for recombinant E3 using the heat shock transformation method. Transformed bacteria were grown in LB/TB medium followed by induction with IPTG (1 mM isopropyl-1-thio-D-galactopyranoside), which was incubated overnight at 15 °C in a Lex System. Then cells were lysed chemically and

physically, and the soluble fraction was separated from insoluble components by centrifugation. His-tag ApoE3 was isolated with nickel-NTA beads eluting with a 250 mM imidazole solution in buffer, which was subsequently dialyzed against 10 mM Tris pH 7.5 and 500 mM NaCl overnight. To facilitate cleavage of His-tag protein, E3 was complexed with dimyristoylphosphatidylcholine at a 13:1 mass ratio of lipid/protein at 24 °C overnight. The protein was then cleaved with thrombin (Sigma-Aldrich, Oakville, ON), and the resultant complex was lyophilized. The protein was extracted from the complex by organic extraction using a chloroform/methanol (2:1 v/v) solution. The organic solvent was aspirated, and the precipitated protein was redissolved in 6 M urea before passing through a nickel column to remove cleaved His-tags. The final product was checked for purity by SDS-PAGE, lyophilized, and stored at −20 °C until use.

Formulation of Porphyrin Nanodiscs. Porphyrin nanodiscs were prepared by the detergent dialysis technique. In brief, a thin film was prepared by dissolving pyro-lipid in methanol and dried in a glass tube under a stream of N_2. The dried film was further dried under vacuum for at least 1 h prior to the start of the experiment. A solution of sodium cholate was used to rehydrate the film such that the final sodium cholate concentration was 20 mM. Apolipoproteins were added to each tube so that the final lipid/protein molar ratio varied from 25:1 to 100:1. Once added, the tubes were transferred to 37 °C and incubated with shaking overnight. The formulation was subsequently dialyzed against three changes of PBS (pH 7.5) over 24 h. Time point samples were collected at predetermined intervals and assessed for fluorescence in a microplate fluorometer (Spectramax M5, Molecular Devices, CA) by exciting at 410 nm and collecting emission at 670 nm. PBS was used as the main experimental buffer unless otherwise stated. A control preparation comprising only pyro-lipid was formulated in the same manner as described above with the exception that the apolipoprotein was withheld during the incubation step.

Proteinase K Degradation Experiment. E3 porphyrin nanodiscs were diluted to 83 μM and treated with 11 units of proteinase K dissolved in 50% v/v glycerol or the equivalent volume of 50% (v/v) glycerol. The particle size in solution was measured every two minutes by dynamic light scattering with a scattering angle of 90° at a temperature of 37 °C. Measurement parameters were adjusted to account for changes in the viscosity of water after glycerol addition. A kinetic size curve was generated over 2 h. At the end of the experiment, a small aliquot of the proteinase K treated or control nanodiscs were retained for transmission electron microscopy.

Transmission Electron Microscopy. Nanoparticle formulations were imaged by negative-staining transmission electron microscopy. Ten microliters of nanoparticle solution was applied to a glow-discharged 400 mesh carbon-coated EM grid. The droplet was allowed to sit for 1 min before blotting with filter paper. The residual solution was washed twice by dipping the grid with two drops of ddH2O prior to staining with 2% uranyl acetate for 1 min. The droplet of stain was blotted away, and the grid allowed to air-dry before imaging under the microscope (Hitachi; Gaithersburg, MD). Grids were viewed at an acceleration voltage of 75 keV.

Fluorescence Unquenching Experiment. To measure the extent of quenching in the nanodisc, the fluorescence of 1 μM nanodisc (pyro-lipid concentration) in PBS was measured. A second sample was measured in which 1 μM nanodisc was disrupted by 0.5% TX-100 prepared by adding 20 μL of a 25% (v/v) solution to a final volume of 1 mL. The fluorometer (Horiba Jobin Yvon; Edison, NJ) was set to excite the samples at 410 nm and collect between 600 and 750 nm. The peak intensity was recorded, and the percent quenching was derived by the following equation:

$$\% \text{ quenching} = \left(1 - \frac{F_0}{F_{\text{detergent}}}\right) \times 100$$

where F_0 is the initial quenched fluorescence and $F_{\text{detergent}}$ is the unquenched fluorescence.

Singlet Oxygen Generation Experiments. The degree of singlet oxygen generated in nanodiscs in the quenched and unquenched nanodisc formulations was determined using the

SOSG reagent following manufacturer protocols. SOSG was dissolved in methanol to prepare a 5 mM solution and was prepared fresh at the start of each experiment. A1 porphyrin nanodiscs (1 μM), intact or unquenched with 0.5% Triton X-100, were mixed with SOSG to a final concentration of 6 μM. Samples were treated with an array of light-emitting diodes at 660 nm with a fluence rate of 1.7 mW/cm^2. At 0.5 J intervals, SOSG fluorescence was measured by exciting at 500 nm and collecting between 520 and 600 nm. There was no detectable pyro-lipid fluorescence within this emission window.

Cell Uptake Studies. ldlA7 and ldlA[mSRBI] were cultured in Ham's F-12 medium supplemented with 2 mM L-glutamine, 1% streptomycin/penicillin, and 5% fetal bovine serum. In addition, the ldlA[mSRBI] culture medium was supplemented with 400 μg/mL G418. Forty-thousand ldlA7 and ldlA[mSRBI] cells were seeded in eight-well chamber slides 24 h prior to the start of the study. To begin the cell uptake studies, cells were incubated with nanodiscs (2.4 μM, pyro-lipid concentration) for 3 h. The cells were then washed three times with PBS, fixed, and imaged by confocal microscopy.

Collagen Gel Diffusion Studies. Collagen gels were prepared as described previously with slight modification.[30] To an Eppendorf tube, 665.6 μL of type I rat tail collagen (11.43 mg/mL) was combined with 194 μL of ddH2O, 117.6 μL of EDTA (0.17 M), and 23 μL of NaOH (1 M). The gel was maintained at 4 °C until polymerization was initiated. The well-mixed solution was carefully applied to glass capillary tubes (Vitrocom; Mountain Lakes, NJ) such that 3.5 cm of the tube was filled. The gel was layered with approximately 20 μL of ddH2O, sealed with a resin, and polymerized at 37 °C for 3 h. After polymerization, the resin was removed and porphyrin nanodiscs or porphysomes were loaded into each tube (20 μL; 200 μM; $n = 3$ per group), resealed, and incubated at 37 °C for 14 h. Fluorescent images from each sample were captured, and line profiles were drawn across the tube using ImageJ. The normalized fluorescence intensity as a function of distance was fit to a one-dimensional diffusion model using the following equation:[30]

$$C(x, t) = a \operatorname{erfc}\left(\frac{x}{2\sqrt{Dt}}\right) + b$$

where t is the incubation time (s), x is the distance along the gel (cm), erfc is the complementary error function, and a and b are the constants for the fitted equation. Data were fitted using Graphpad Prism 5.0 (La Jolla, CA).

REFERENCES AND NOTES

1. Huynh, E.; Zheng, G. Engineering Multifunctional Nanoparticles: All-in-One *versus* One-for-All. *WIREs Nanomed. Nanobiotechnol.* **2013**, 10.1002/wnan.1217.
2. McCarthy, J. R.; Perez, J. M.; Brückner, C.; Weissleder, R. Polymeric Nanoparticle Preparation That Eradicates Tumors. *Nano Lett.* **2005**, *5*, 2552–2556.
3. Zheng, G.; Chen, J.; Stefflova, K.; Jarvi, M.; Li, H.; Wilson, B. C. Photodynamic Molecular Beacon as an Activatable Photosensitizer Based on Protease-Controlled Singlet Oxygen Quenching and Activation. *Proc. Natl. Acad. Sci. U.S.A.* **2007**, *104*, 8989–8994.

4. Kim, H.; Mun, S.; Choi, Y. Photosensitizer-Conjugated Polymeric Nanoparticles for Redox-Responsive Fluorescence Imaging and Photodynamic Therapy. *J. Mater. Chem. B* **2013**, *1*, 429–431.

5. Lovell, J. F.; Jin, C. S.; Huynh, E.; Jin, H.; Kim, C.; Rubinstein, J. L.; Chan, W. C.; Cao, W.; Wang, L. V.; Zheng, G. Porphysome Nanovesicles Generated by Porphyrin Bilayers for Use as Multimodal Biophotonic Contrast Agents. *Nat. Mater.* **2011**, *10*, 324–332.

6. Lovell, J. F.; Jin, C. S.; Huynh, E.; Macdonald, T. D.; Cao, W.; Zheng, G. Enzymatic Regioselection for the Synthesis and Biodegradation of Porphysome Nanovesicles. *Angew. Chem., Int. Ed.* **2012**, 2429–2433.

7. Liu, T. W.; MacDonald, T. D.; Shi, J.; Wilson, B. C.; Zheng, G. Intrinsically Copper-64-Labeled Organic Nanoparticles as Radiotracers. *Angew. Chem., Int. Ed.* **2012**, *51*, 13128–13131.

8. Jin, C. S.; Lovell, J. F.; Chen, J.; Zheng, G. Ablation of Hypoxic Tumors with Dose-Equivalent Photothermal, but Not Photodynamic, Therapy Using a Nanostructured Porphyrin Assembly. *ACS Nano* **2013**, 10.1021/nn3058642.

9. Jain, R. K.; Stylianopoulos, T. Delivering Nanomedicine to Solid Tumors. *Nat. Rev. Clin. Oncol.* **2010**, *7*, 653–664.

10. Cabral, H.; Matsumoto, Y.; Mizuno, K.; Chen, Q.; Murakami, M.; Kimura, M.; Terada, Y.; Kano, M. R.; Miyazono, K.; Uesaka, M.; *et al*. Accumulation of Sub-100 nm Polymeric Micelles in Poorly Permeable Tumours Depends on Size. *Nat. Nanotechnol.* **2011**, *6*, 815–823.

11. Pluen, A.; Boucher, Y.; Ramanujan, S.; McKee, T. D.; Gohongi, T.; di Tomaso, E.; Brown, E. B.; Izumi, Y.; Campbell, R. B.; Berk, D. A.; *et al*. Role of Tumor−Host Interactions in Interstitial Diffusion of Macromolecules: Cranial *vs.* Subcutaneous Tumors. *Proc. Natl. Acad. Sci. U.S.A.* **2001**, *98*, 4628–4633.

12. Lichtenberg, D.; Freire, E.; Schmidt, C. F.; Barenholz, Y.; Felgner, P. L.; Thompson, T. E. Effect of Surface Curvature on Stability, Thermodynamic Behavior, and Osmotic Activity of Dipalmitoylphosphatidylcholine Single Lamellar Vesicles. *Biochemistry* **1981**, *20*, 3462–3467.

13. Bricarello, D. A.; Smilowitz, J. T.; Zivkovic, A. M.; German, J. B.; Parikh, A. N. Reconstituted Lipoprotein: A Versatile Class of Biologically-Inspired Nanostructures. *ACS Nano* **2011**, *5*, 42–57.

14. Ritchie, T. K.; Grinkova, Y. V.; Bayburt, T. H.; Denisov, I. G.; Zolnerciks, J. K.; Atkins, W. M.; Sligar, S. G. Chapter 11 - Reconstitution of Membrane Proteins in Phospholipid Bilayer Nanodiscs. *Methods Enzymol.* **2009**, *464*, 211–231.

15. Cormode, D. P.; Chandrasekar, R.; Delshad, A.; Briley-Saebo, K. C.; Calcagno, C.; Barazza, A.; Mulder, W. J.; Fisher, E. A.; Fayad, Z. A. Comparison of Synthetic High Density Lipoprotein (HDL) Contrast Agents for MR Imaging of Atherosclerosis. *Bioconjugate Chem.* **2009**, *20*, 937–943.

16. Murakami, T.; Wijagkanalan, W.; Hashida, M.; Tsuchida, K. Intracellular Drug Delivery by Genetically Engineered High-Density Lipoprotein Nanoparticles. *Nanomed* **2010**, *5*, 867–879.

17. Ng, K. K.; Lovell, J. F.; Zheng, G. Lipoprotein-Inspired Nanoparticles for Cancer Theranostics. *Acc. Chem. Res.* **2011**, *44*, 1105–1113.

18. Oda, M. N.; Hargreaves, P. L.; Beckstead, J. A.; Redmond, K. A.; van Antwerpen, R.; Ryan, R. O. Reconstituted High Density Lipoprotein Enriched with the Polyene Antibiotic Amphotericin B. *J. Lipid Res.* **2006**, *47*, 260–267.

19. Shahzad, M. M.; Mangala, L. S.; Han, H. D.; Lu, C.; Bottsford-Miller, J.; Nishimura, M.; Mora, E. M.; Lee, J. W.; Stone, R. L.; Pecot, C. V.; *et al*. Targeted Delivery of Small Interfering RNA Using Reconstituted High-Density Lipoprotein Nanoparticles. *Neoplasia* **2011**, *13*, 309–319.

20. Matz, C. E.; Jonas, A. Micellar Complexes of Human Apolipoprotein a-I with Phosphatidylcholines and Cholesterol Prepared from Cholate-Lipid Dispersions. *J. Biol. Chem.* **1982**, *257*, 4535–4540.

21. van Antwerpen, R.; Chen, G. C.; Pullinger, C. R.; Kane, J. P.; LaBelle, M.; Krauss, R. M.; Luna-Chavez, C.; Forte, T. M.; Gilkey, J. C. Cryo-Electron Microscopy of Low Density Lipoprotein and Reconstituted Discoidal High Density Lipoprotein: Imaging of the Apolipoprotein Moiety. *J. Lipid Res.* **1997**, *38*, 659–669.

22. Segrest, J. P.; De Loof, H.; Dohlman, J. G.; Brouillette, C. G.; Anantharamaiah, G. M. Amphipathic Helix Motif: Classes and Properties. *Proteins: Struct., Funct., Bioinf.* **1990**, *8*, 103–117.

23. Jayaraman, S.; Gantz, D. L.; Gursky, O. Kinetic Stabilization and Fusion of Apolipoprotein a-2:Dmpc Disks: Comparison with Apoa-1 and Apoc-1. *Biophys. J.* **2005**, *88*, 2907–2918.

24. Leng, J.; Egelhaaf, S. U.; Cates, M. E. Kinetics of the Micelle-to-Vesicle Transition: Aqueous Lecithin-Bile Salt Mixtures. *Biophys. J.* **2003**, *85*, 1624–1646.

25. Flors, C.; Fryer, M. J.; Waring, J.; Reeder, B.; Bechtold, U.; Mullineaux, P. M.; Nonell, S.; Wilson, M. T.; Baker, N. R. Imaging the Production of Singlet Oxygen *in Vivo* Using a New Fluorescent Sensor, Singlet Oxygen Sensor Green®. *J. Exp. Bot.* **2006**, *57*, 1725–1734.

26. Xu, S.; Laccotripe, M.; Huang, X.; Rigotti, A.; Zannis, V. I.; Krieger, M. Apolipoproteins of HDL Can Directly Mediate Binding to the Scavenger Receptor SR-BI, an HDL Receptor That Mediates Selective Lipid Uptake. *J. Lipid Res.* **1997**, *38*, 1289–1298.

27. Popović, Z.; Liu, W.; Chauhan, V. P.; Lee, J.; Wong, C.; Greytak, A. B.; Insin, N.; Nocera, D. G.; Fukumura, D.; Jain, R. K.; *et al*. A Nanoparticle Size Series for *in Vivo* Fluorescence Imaging. *Angew. Chem., Int. Ed.* **2010**, *49*, 8649–8652.

28. Chauhan, V. P.; Popovic, Z.; Chen, O.; Cui, J.; Fukumura, D.; Bawendi, M. G.; Jain, R. K. Fluorescent Nanorods and Nanospheres for Real-Time *in Vivo* Probing of Nanoparticle Shape-Dependent Tumor Penetration. *Angew. Chem., Int. Ed.* **2011**, *50*, 11417–11420.

29. Ramanujan, S.; Pluen, A.; McKee, T. D.; Brown, E. B.; Boucher, Y.; Jain, R. K. Diffusion and Convection in Collagen Gels: Implications for Transport in the Tumor Interstitium. *Biophys. J.* **2002**, *83*, 1650–1660.

30. Tong, R.; Hemmati, H. D.; Langer, R.; Kohane, D. S. Photoswitchable Nanoparticles for Triggered Tissue Penetration and Drug Delivery. *J. Am. Chem. Soc.* **2012**, *134*, 8848–8855.

31. Cao, W.; Ng, K. K.; Corbin, I.; Zhang, Z.; Ding, L.; Chen, J.; Zheng, G. Synthesis and Evaluation of a Stable Bacteriochlorophyll-Analog and Its Incorporation into High-Density Lipoprotein Nanoparticles for Tumor Imaging. *Bioconjugate Chem.* **2009**, *20*, 2023–2031.

32. Zaiou, M.; Arnold, K. S.; Newhouse, Y. M.; Innerarity, T. L.; Weisgraber, K. H.; Segall, M. L.; Phillips, M. C.; Lund-Katz, S. Apolipoprotein E−Low Density Lipoprotein Receptor Interaction. Influences of Basic Residue and Amphipathic α-Helix Organization in the Ligand. *J. Lipid Res.* **2000**, *41*, 1087–1095.